Final Technical Report

USGS Award Nos. G23AP00396 and G23AP00397

HVSR Site Terms for Nonergodic Ground Motion Models: Collaborative Research with Tufts University and Merrimack College

Laurie G. Baise, Professor and Chair
Dept. of Civil and Env. Engineering, Tufts University, 200 College Ave, Medford, MA, 02155
617-627-2211, 617-627-3994, laurie.baise@tufts.edu

James Kaklamanos, Professor
Dept. of Civil Engineering, Merrimack College, 315 Turnpike Street, North Andover, MA, 01845
978-837-3401, KaklamanosJ@merrimack.edu

Maggie Roberts, Graduate Student Researcher
Dept. of Civil and Env. Engineering, Tufts University, 200 College Ave, Medford, MA, 02155
774-225-8225, maggie.roberts@tufts.edu

Shiying Nie, Postdoctoral Researcher
Dept. of Civil and Env. Engineering, Tufts University, 200 College Ave, Medford, MA, 02155
858-405-2727, shiying.nie@tufts.edu

Weiwei Zhan, Assistant Professor
Dept. of Civil, Env. and Construction Engineering, University of Central Florida, 4000 Central Florida Blvd, Orlando, FL, 32816
407-823-1361, Weiwei.Zhan@ucf.edu

Project Term: 1 August 2023 – 31 July 2024

Acknowledgment of Support and Disclaimer:

This material is based upon work supported by the U.S. Geological Survey under Grant Nos. G23AP00396 and G23AP00397. The views and conclusions contained in this document are those of the authors and should not be interpreted as representing the opinions or policies of the U.S. Geological Survey. Mention of trade names or commercial products does not constitute their endorsement by the U.S. Geological Survey.

Abstract

This study presents a correction factor for ground-motion model (GMM) site terms in California derived from horizontal-to-vertical spectral ratio (HVSR) data. Spatially continuous, non-ergodic models are becoming a popularized method for GMM development. We propose enhancing these models with local geotechnical information, i.e., HVSR data, when it is available. The model was developed from microtremor-based (mHVSR) data from the Wang et al. (2022) Horizontal-to-Vertical Spectral Ratio Database, and earthquake ground motion-based (eHVSR) data from the Ji et al. (2022) DesignSafe Ground Motion Database. The HVSR data were processed and classified as either having a clear fundamental resonance peak, being flat with no fundamental resonance at the site, or failing to meet either of these classifications. The fundamental resonance frequency, amplitude, and half-power bandwidth parameters were derived from the passing HVSRs. The consistency between the eHVSR and mHVSR curves was assessed for both the HVSR classification and parameter extraction at passing stations. The classification of the HVSR data and the HVSR parameters at stations with a fundamental resonance frequency are analyzed for their ability to reduce intersite (site-to-site) variability of peak ground acceleration (PGA), peak ground velocity (PGV), and pseudo-spectral accelerations from 0.01 to 10 seconds. The ground-motion parameters are decomposed from the residuals of the Boore et al. (2014) (BSSA14) GMM, modified with a non-ergodic geospatial based site term (Roberts et al., 2024). Two sets of models are compared, ones that are fit using mHVSR data only, and ones that are fit using a weighted combination of mHVSR and eHVSR data, based on the added variability when using eHVSR to fit a model intended for use with mHVSR site parameters. A novel correction factor is developed that uses a linear term for passing stations based on the fundamental peak frequency of the site, fit using mHVSR and eHVSR data, and a constant correction factor for sites with a flat mHVSR curve defined by our proposed flat criteria. The HVSR correction factor shows a reduction in site-to-site variability across all frequencies compared to the non-ergodic geospatial-based site terms with no correction factors. This study illustrates the effectiveness of using HVSR data to enhance site effects models, and highlights the potential for gaining site information from both eHVSR and mHVSR data, considering stations that have clear fundamental resonance frequencies and those that do not.

Table of Contents

1. Introduction

Horizontal-to-vertical spectral ratios (HVSRs, Nogoshi and Igarashi 1971; Nakamura 1989) are an on-site technique for analyzing site effects. The HVSR is computed as the ratio of the amplitude spectrum of the horizontal components to the amplitude spectrum of the vertical component, using recordings from either microtremors or earthquake ground motions (termed as mHVSR and eHVSR, respectively). HVSR is predominantly used for approximating the site fundamental frequency f_0 from the fundamental resonance peak of the HVSR (Nakamura, 1989). It is widely recognized that HVSRs are adequate at predicting the site fundamental frequency but not the corresponding amplitude (Nakamura, 1989; Lermo and Chávez-García, 1993; Carpenter et al., 2020).

The Site Effects Assessment Using Ambient Excitations (SESAME) project, a European Commission contract to build consensus on HVSR use guidelines, provides a set of criteria for determining if an HVSR curve has a clear peak. SESAME outlines a set of criteria for both reliability of the HVSR curves and the clarity of the peak that need to be met to identify a resonance peak from an HVSR recording. The SESAME criteria ensure that peak detection is a standardized process across studies (SESAME, 2004).

Utilizing HVSR to determine f_0 has been particularly useful in classifying site response in resonant sediments due to its simplicity and low cost (Lermo and Chávez-Garcia, 1993; Carpenter et al., 2018; Zhu et al., 2020). Additionally, the use of f_0 as a predictor variable to estimate site effects in GMMs has shown success in locations globally (eg., Braganza et al., 2016; Gallipoli and Mucciarelli, 2009; Hassani and Atkinson, 2016, 2018; Yazdi et al., 2023). These models utilize the f_0, and in some cases the amplitude of the peak, but do not leverage the full power of HVSR data. In this work, we extract parameters from both eHVSR and mHVSR curves to present an analysis of information that can be gained from both eHVSR and mHVSR with the goal of using both to develop a GMM site term correction factor. The parameters evaluated are the frequency of the fundamental resonance peak, peak amplitude, and the half-power bandwidth (HPB, the difference between the frequencies corresponding to $1/\sqrt{2}$ * peak amplitude), shown in Figure 1, as well as a new classification system that defines flat recordings.

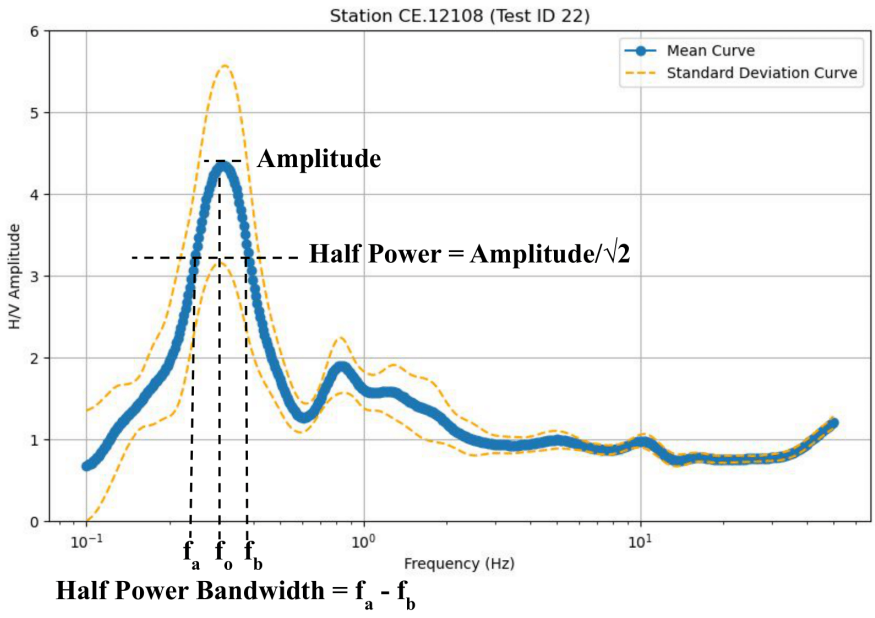

Figure 1. Illustration of HVSR parameters evaluated in this study: fundamental resonance peak (f_0), peak amplitude, and the half-power bandwidth (HPB) (bounded by the frequencies f_a and f_b).

The correlation and differences between obtaining HVSR curves from earthquake ground motions and from microtremors have been documented in the literature. Results from mHVSR have been shown to be able to be corrected to eHVSR in Japan (Kawase et al. 2019). Similarly, in California, the f_0 derived from eHVSR was found to scale linearly with mHVSR measurements up to 300 meters away (Hassani et al., 2019). However, despite the correlation between the two measurements, they are not always equal at a site. Comparisons of peak frequencies of eHVSR and mHVSR obtained in California show that 68% of observed flat eHVSR resonances were also flat for mHVSR, and 85% of observed eHVSR with at least one clear resonance also had at least one clear resonance for mHVSR (Vantassel et al., 2024). This presents a challenge when trying to create and utilize HVSR datasets, particularly for developing ground motion models (GMMs), because the two methods do not always produce equivalent results. Despite differences in the two recording types, models developed for Taiwan showed that for PGA, station terms developed for mHVSR were comparable to terms developed for eHVSR (Choa et al., 2021). The body of work surrounding eHVSR and mHVSR suggests that while the two recordings are not always equivalent, there is correlation and a level of consistency between the two. We consider this correlation and the known inequalities for our study in California.

We have previously developed a geospatial-based site term for use with NGA-West2 GMMs (Roberts et al., 2024). This model uses continuously available geospatial parameters (regional geologic unit and topographic position index) to estimate the linear soil amplification term. Geotechnical information, such as HVSR data, should be added to this model when available to improve its accuracy. This study investigates the use of HVSR to correct the GMM site terms with local site data. We look to extract the greatest amount of site information possible from HVSR curves by investigating the relationship between eHVSR and mHVSR curves, developing a classification system for flat curves, and examining multiple HVSR parameters (f_0, amplitude, and half-power bandwidth) to inform development of comprehensive HVSR site terms for use with GMMs in California.

2. Data and Methods

eHVSR Data and Processing

Earthquake ground motions were obtained from the Ji et al. (2022) DesignSafe Ground Motion Database (DSGMD). Ground motions in the DSGMD were queried from the USGS Comprehensive Catalog (ComCat; Guy et al., 2015). The DSGMD contains more than 287,804 processed ground motions from 2,641 earthquakes recorded at 3,709 stations in and near California from 1999 to 2021. For this study, we only used stations that are located in California and have at least four earthquake recordings, in order to produce reasonable mean and standard deviation statistics of eHVSR curves, resulting in 1,658 processed stations. Earthquake recordings were measured by both accelerometers (43% of stations) and velocimeters (57% of stations). Figure 2 shows the spatial distribution of the selected stations for computing eHVSR.

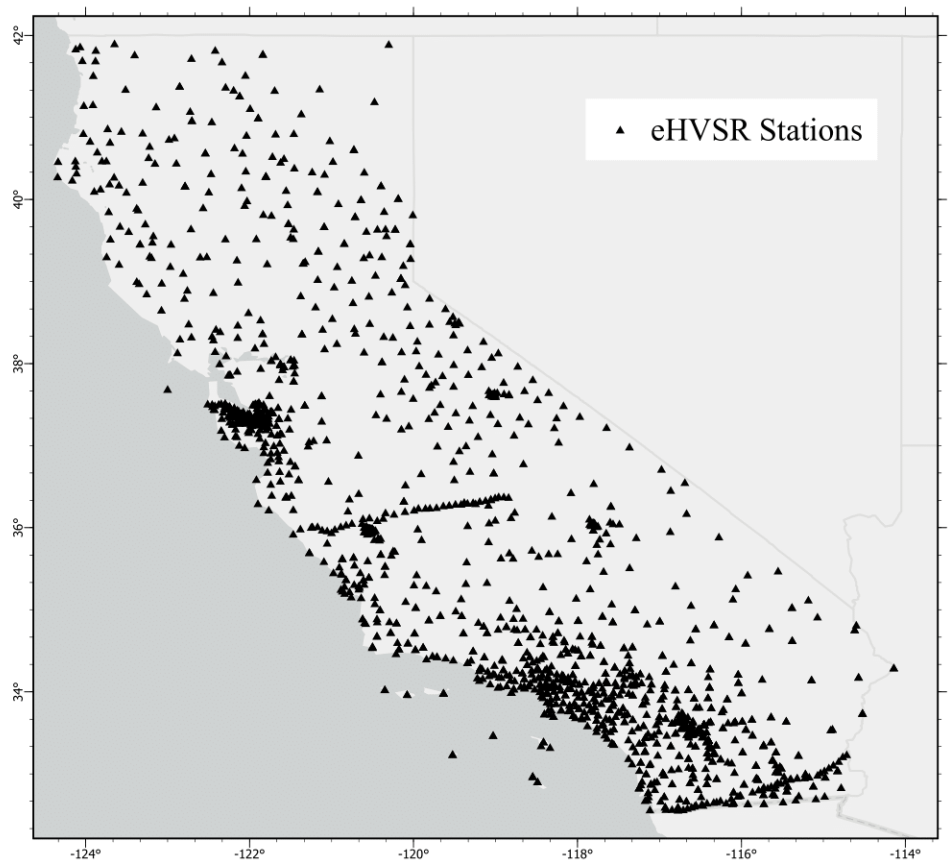

Figure 2. eHVSR station locations for the study area in California.

The pre-processed ground motions were downloaded from the DSGMD and then processed using *hvsrpy* (Vantassel, 2020). *Hvsrpy* is an open-source Python package for processing eHVSR and mHVSR data. The full earthquake record was processed for each recording at all stations. The ground motions were processed using a 20% Tukey window (10% off either end) in the time domain, smoothing the horizontal and vertical spectra using a Konno and Ohmachi (1998) window with a coefficient (b) of 40, resampling between 0.4 and 10 Hz with 128 points on a logarithmic scale, and combining the horizontal components using the geometric mean. To account for differences in sampling rates between earthquakes, frequency domain resampling was performed, and to account for differences in orientation, all earthquake recordings were rotated to magnetic north using *hvsrpy*. These processing settings are consistent with prior eHVSR processing performed in California (Vantassel et al., 2024).

The fully automated frequency-domain window-rejection algorithm (Cox et al., 2020) in *hvsrpy* was then applied to all the processed stations. The window-rejection algorithm increases HVSR data quality by rejecting windows with extreme f_0 values that are not representative of the site conditions and are instead contaminated by factors such as variability from ambient noise and environmental conditions. The median and standard deviation values of HVSR were then calculated using all valid waveform windows, assuming a log-normal distribution; this is consistent with the methodology proposed by SESAME (2004) and Cox et al. (2020).

The SESAME criteria were then applied using *hvsrpy* to the log-normal median and standard deviation curves to identify if a clear peak could be determined for each station. The SESAME guidelines require

passing the three reliability criteria and at least five of the six clarity criteria in order to verify a clear peak. These guidelines were strictly followed for all eHVSR stations. The fundamental resonance peak, peak amplitude, and half-power bandwidth parameters were extracted for all stations with a clear peak using *hvsrpy*. A schematic of the window processing and parameter extraction is shown in Figure 3 (modified from the *hvsrpy* output). Passing peaks were identified at 252 stations, and 1,406 stations failed to have a peak identified.

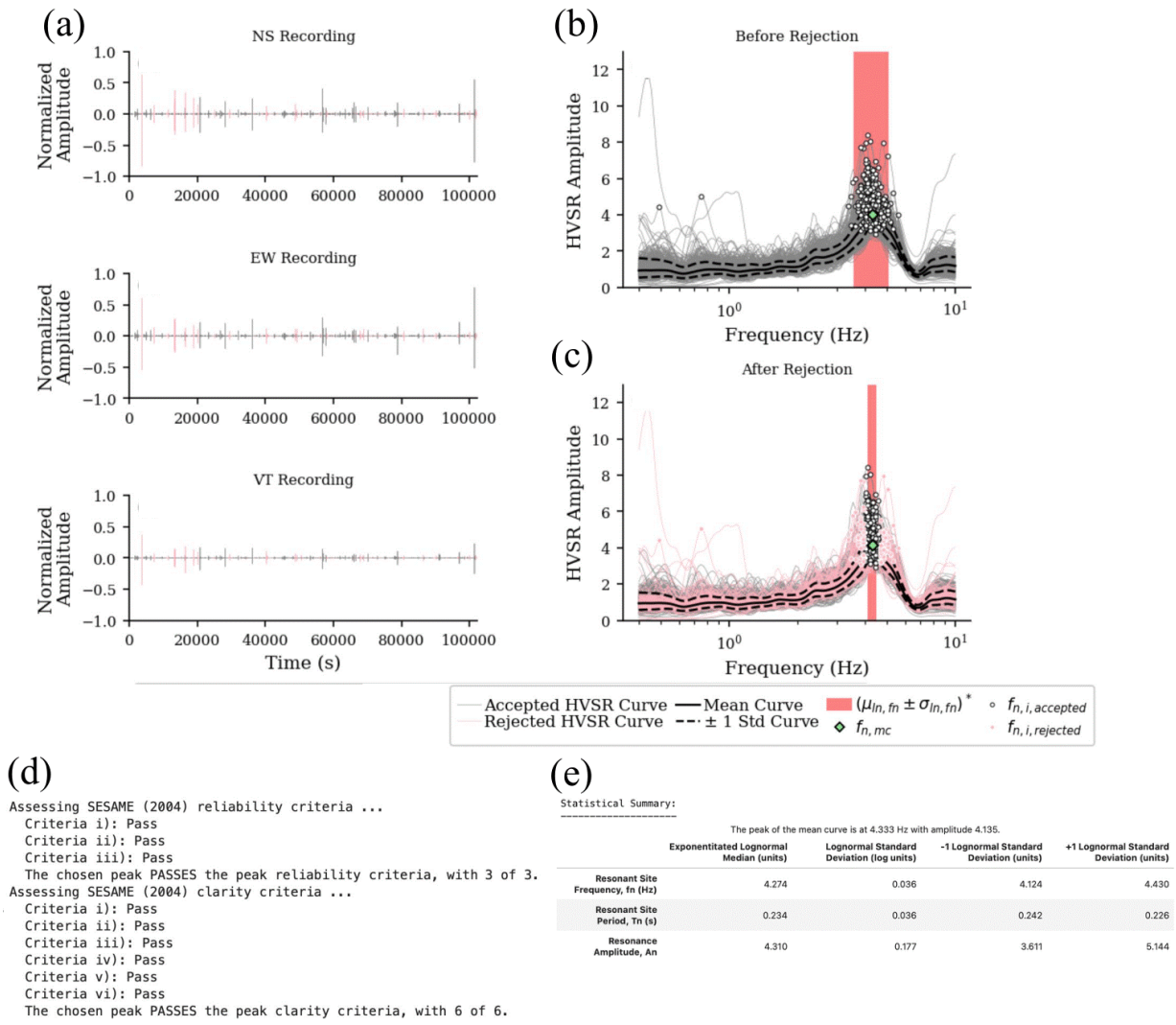

Figure 3. eHVSR processing schematic for a station, including: (a) the horizontal and vertical components of the recordings, (b) all processed recordings, (c) the windows identified for rejection and accepted windows with the mean and standard deviation curves, (d) the SESAME criteria, and (e) the resulting peak and amplitude parameters. This figure was adapted from *hvsrpy* output (Vantassel, 2020).

mHVSR Data and Processing

Microtremor HVSR data were obtained from a subset of the Wang et al. (2022) Horizontal-to-Vertical Spectral Ratio Database, accessed via DesignSafe. The database is part of a larger effort by the California Strong Motion Instrumentation Program (CSMIP) to create a reliable site parameter database. The database is a relational database that provides mean and standard deviation HVSR curves, as well as station and recording information for 1423 microtremor recordings at 703 stations, primarily in California. Figure 4 shows the spatial distribution of the subset of the dataset used for this study, which includes the 848 recordings from the 490 stations located in California at earthquake seismic stations. The number of recordings per station ranges from one to six.

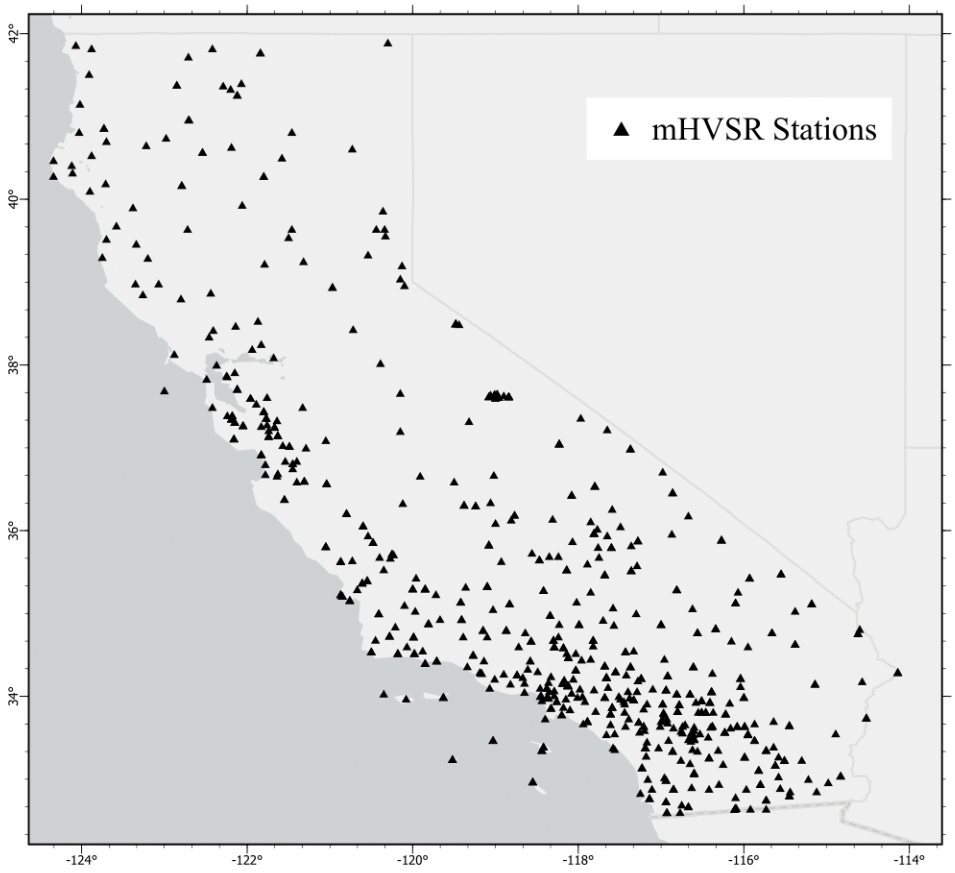

Figure 4. mHVSR station locations for the study area in California.

The recordings are obtained from three-component seismometers (both temporary and permanent) that record microtremor ground vibrations. Microtremor recordings were processed using the processing package *hvsrProc* (Wang, 2021) when time-series data were available (most recordings) and using the open source Geopsy software (Wathelet et al, 2020) on all other recordings to produce the mean and standard deviation curves available in the database. Using the station mean mHVSR curves and their associated standard deviations, the SESAME criteria were applied to identify if a clear peak could be determined for each station. The peak frequencies, peak amplitudes, and the half-power bandwidth parameters were extracted for all mHVSR stations with a clear peak using *hvsrpy*. Passing peaks were identified for 211 recordings, and 637 recording failed to have a peak identified.

HVSR-based Seismic Site Classification

In the case of both eHVSR and mHVSR in California, the majority of HVSR recordings fail to have a clear resonance peak identified. In this study, 85% of eHVSR and 75% of mHVSR recordings failed to have a peak identified. This is due in part to the number of sites across the state that are located on deep soil profiles without a strong impedance contrast, or stations that are located on rock. On the other hand, there are some stations that fail to have a peak identified due to the variability and inconsistency in HVSR measurements from ambient noise and environmental conditions. We look to identify these stations that do not have an impedance contrast and would consistently not produce a clear HVSR peak, and separate them from HVSR recordings that fail to have a peak identified due to the variability and inconsistency in HVSR measurements.

In previous HVSR studies, recordings have been deemed "flat" if they fail to have a clear peak identified. In this study, we make a distinction between (a) recordings that are completely flat with no peaks present, and (b) recordings that failed to have a clear peak identified (using SESAME criteria), but are not completely flat (i.e. a peak that is too wide, not distinct enough, or has too high a standard deviation to be classified as a clear peak). We view the failed non-flat HVSR data as being inconclusive (i.e., it would be difficult to glean and site information). However, the failed flat HVSR data do tell us information about the site characteristics and the lack of impedance contrast at the site. Classifying a subset of failing HVSR measurements as flat allows us to gain insights about site characterization and inform GMMs from both recordings with a passing fundamental resonance peak, as well as recordings that are flat. Additionally, by removing the recordings that do not produce reliable results (i.e., failed, but not flat recordings), we are better able to determine the extent to which eHVSR and mHVSR match at a given site.

Recordings were determined to be flat if they failed SESAME clarity Criteria 1 and 2 and had a peak H/V amplitude below 1.5. These criteria are outlined in Figure 5. Criteria 1 and 2 involve the height of the peak being tested relative to the curve around it; a height of half the amplitude must not be reached within half the peak frequency to the peak frequency (Criteria 1) and within the peak frequency to four times the peak frequency (Criteria 2). These indicate either that the "peak" being assessed is not tall compared to the surrounding record, or that the curve does not taper down in amplitude within the required range. Criteria 3 states that the peak amplitude must be less than 1.5, which is similar to SESAME clarity criteria 3 (the peak amplitude must be above 2), but stricter in order to identify the completely flat curves. Passing all three of these criteria indicates that the curve is relatively flat when comparing the peak to its surrounding (Criteria 1 and 2) and does not have a section of high amplitude (Criteria 3).

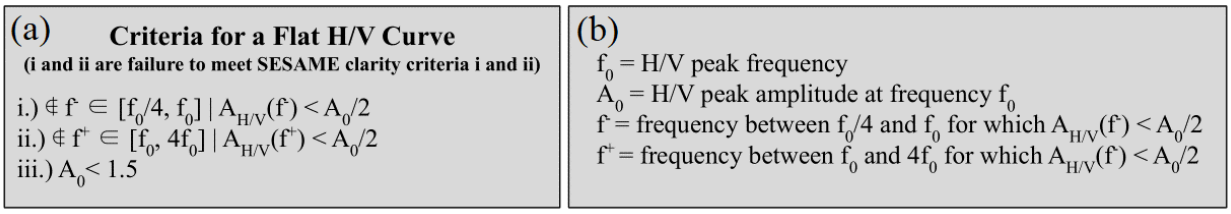

Figure 5. (a) Criteria implemented to identify a flat HVSR curve, and (b) definitions of variables in the criteria.

These three criteria for identifying flat HVSR curves provide a systematic way to classify flat eHVSR and mHVSR recordings. This method also has a level of consistency and ease of implementation by being based upon the widely used SESAME criteria. When applied to this dataset, 120 out of the 1406 eHVSR stations without an identified clear peak were classified as flat. For mHVSR, 76 of the 637 failed recordings were classified as flat. Figure 6 showcases the difference between recordings that meet the flat criteria and ones that do not have a passing peak, but also do not meet the flat criteria.

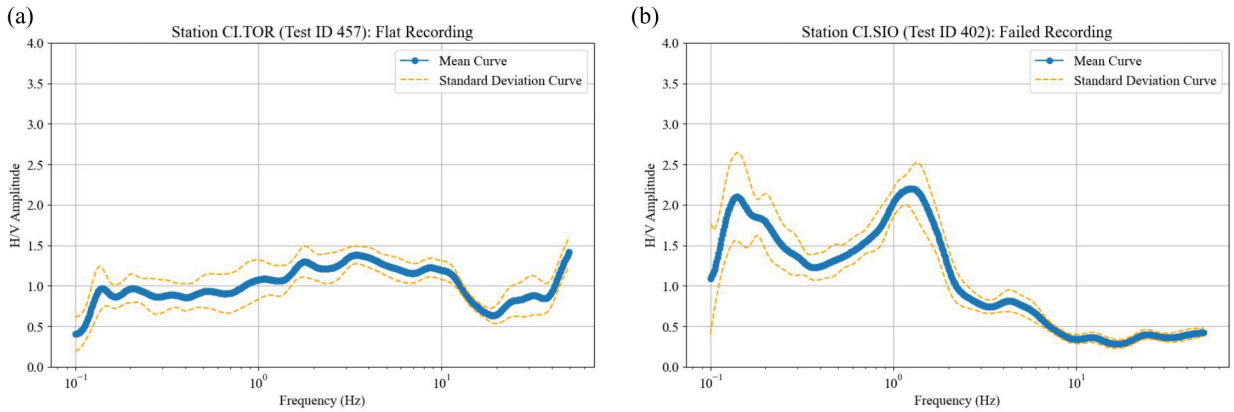

Figure 6. mHVSR recordings that both failed to have a clear peak identified: (a) a recording classified as flat, and (b) a recording that failed to be classified as flat.

Final Dataset

The final dataset used for analysis includes the three station classifications of pass (a clear fundamental resonance peak identified), flat (meet the three failing criteria), and fail (no clear peak identified, but did not meet the flat criteria). Stations with passing peaks have f_0, amplitude, and HPB parameters identified for each station. Table 1 summarizes the distribution of the dataset for both eHVSR station and mHVSR recording classifications, and Figure 7 shows their geographic distribution.

Table 1. eHVSR and mHVSR dataset distribution by recording classification.

Classification	Pass	Flat	Fail	Total
eHVSR	252	120	1286	1658
mHVSR	211	76	561	848

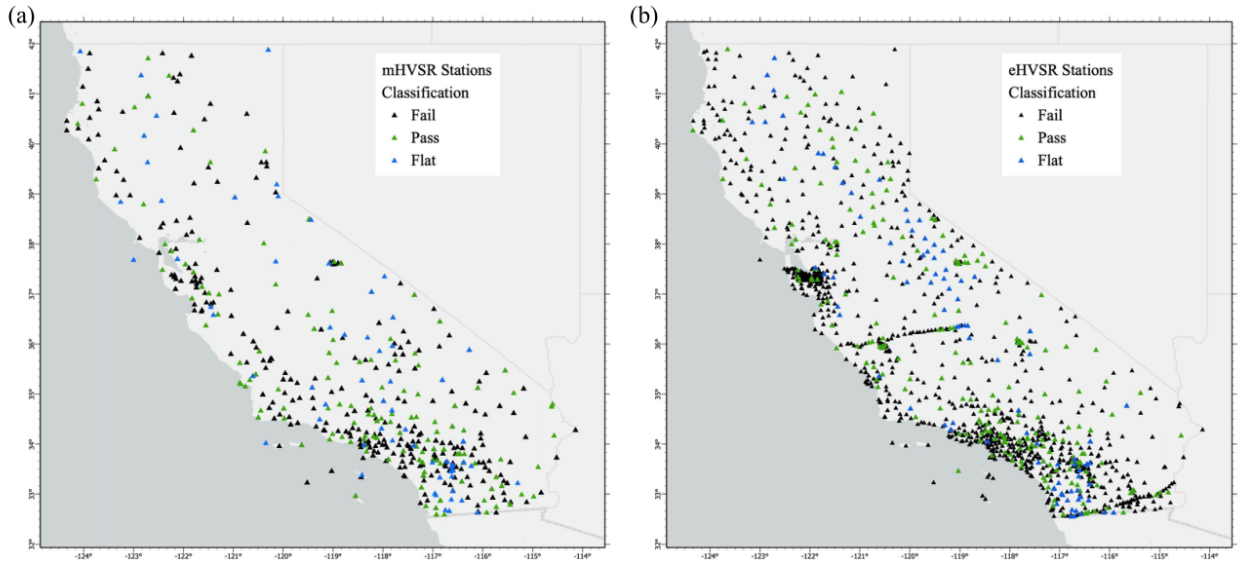

Figure 7. Geographic distribution of station classifications for (a) mHVSR and (b) eHVSR.

Ground Motion Model Residuals

In order to develop an HVSR-based correction for GMM site terms, the ground motions from the DesignSafe Ground Motion Database (Ji et al., 2022) at the sites in our HVSR final dataset were evaluated using BSSA14 GMM (Boore et al. 2014) modified with the geospatial site term we previously developed (Roberts et al., 2024). This model was selected because the geospatial site term utilizes only continuous variables (regional geologic unit and topographic position index (TPI)) to generate a site term. While the geospatial-informed model shows a reduction of site-to-site (S2S) variability (7.6% averaged across PGA, PGV and 21 PSAs from 0.01 to 10 seconds) compared to the original model, the geospatial-informed model could be enhanced with site-specific geotechnical measurements, like HVSR, when they are available. The residual (R_{ij}) was calculated for each event (i) at each station (j), as

$$R_{ij,BSSA14\ with\ geospatial\ site\ term} = \ln(Y_{ij}) - \ln(\mu_{ij,BSSA14\ with\ geospatial\ site\ term}), \quad (1)$$

where Y_{ij} is the observed ground motion IM for event i at station j; and μ_{ij} is the corresponding median ground motion IM predicted using the BSSA14 model with the modified site term. We then decompose the ground motion residuals using linear mixed-effects regression (Abrahamson and Youngs, 1992), as

$$R_{ij,BSSA14} = c + \delta E_i + \delta S2S_j + \varepsilon_{ij}, \quad (2)$$

where c, δE_i, $\delta S2S_j$, and ε_{ij} are the bias, event term, site-to-site term, and remaining residual, respectively. The event term, site-to-site term (S2S), and remaining residuals are usually assumed to be normally distributed with zero mean and standard deviations of τ_E, ϕ_S, and σ, respectively. These calculations are performed across PGA, PGV, and PSA for 21 periods from 0.01 to 10 s. The $\delta S2S_j$ term is used as the target variable for fitting the HVSR based correction factor.

Ordinary and Weighted Least Squares Regression

We derived two sets of empirical models to predict S2S in California. The first set of models uses only mHVSR data from passing and flat stations. The mHVSR-based models are produced by fitting each HVSR parameter to the linear functional form in Equation 3 using ordinary least squares (OLS) regression:

$$\delta S2S_j, = \begin{cases} \beta_0 + \boldsymbol{\beta_1 X} + \varepsilon_j, & HVSR\ station\ claasification = pass \\ \alpha + \varepsilon_j, & HVSR\ station\ classification = flat \end{cases}, \quad (3)$$

where β_0 is a constant, $\boldsymbol{\beta_1}$ is a vector of regression coefficients, **X** is a vector of the HVSR parameters, ε_j is the remaining residual, and α is a constant derived from the average $\delta S2S_j$ of the flat stations.

The second set of models uses both mHVSR and eHVSR parameters from passing stations. The models are produced using weighted least squares (WLS) regression. WLS regression allows linear regression to be performed, but accounts for the unequal variance of data points by assigning weights to them. In this case, weights are assigned differently to mHVSR and eHVSR data based on their reliability. eHVSR data is considered surrogate data with higher variance, as inconsistencies often exist between eHVSR and mHVSR parameters at the same station, so it receives a lower weight. This weight for eHVSR data is set using the Nash–Sutcliffe Efficiency Coefficient (E, Nash and Sutcliffe, 1970). The coefficient of efficiency is computed as,

$$E = 1 - \left[\frac{\sum_{i=1}^{N}(Y_i - \widehat{Y}_i)^2}{\sum_{i=1}^{N}(Y_i - \bar{Y})^2}\right] * 100\%\,, \quad (4)$$

where N is the total number of mHVSR and eHVSR pairs, Y_i is the mHVSR parameter (the observed value), $\widehat{Y}_i$ is the eHVSR parameter (the predicted value), and the mean of the mHVSR parameter is denoted by $\bar{Y}$. The coefficient of efficiency measures the goodness of fit relative to the 1-to-1 line, and can range from -∞ to 100%; when E is less than zero, the arithmetic mean of the observed values has greater prediction accuracy than the model itself (Nash and Sutcliffe, 1970). Values of E quantify the agreement between observations and predictions, considering the dispersion of observations and predictions about the 1-to-1 line. The mHVSR data are assigned a weight of one, and eHVSR data are weighted by E to reflect the relative reliability of mHVSR predictions using eHVSR values. The second set of models are developed using WLS to fit Equation (3) with a weight of one for mHVSR data and E for eHVSR data assigned to each parameter evaluated.

We evaluate the performance of alternative regression models by fitting the models to all but 20% of the mHVSR data. The models are then validated on the mHVSR data left out during the regression process. The best model is selected as the model with the lowest root mean square error (RMSE) of the test set of mHVSR data.

3. Results

Flat Station Classification

The stations classified as flat have a distinct geologic and topographic distribution compared to the passing and failed stations. Figure 8 shows the roughness and elevation distributions for the three HVSR-

site groups derived using mHVSR and eHVSR, separately. Roughness and elevation were derived from the GMTED 7.5 arc-second digital elevation model (Danielson and Gesch, 2011). “Flat” sites tend to have higher roughness and elevation values than “Pass” and “Fail” sites. This trend is consistent across mHVSR and eHVSR.

The distribution of the surficial geologic units for each recording classification are shown in Figure 9. The surficial geology of the site was determined using the Wills et al. (2015) surficial geologic unit map for California. The surficial geologic units were then aggregated into broader geologic categories, Quaternary Alluvium (Qal1, Qal2, Qal3, af/Qi, Qi, Qs), Older Alluvium (Qt, Qoa), Tertiary Sediment (Tss, Tsh), Cretaceous-Jurassic Sediment (Kjf, Kss), Crystalline (crystalline), and Volcanic/Metamorphic (Tv, sp). Failing and passing classifications show similar distributions across mHVSR and eHVSR data, consisting of approximately a third of Quaternary Alluvium recordings (31–39%) and approximately a quarter (15–28%) of recordings located in Crystalline or Older Alluvium. On the other hand, flat recordings for both mHVSR and eHVSR data were majority Crystalline (54% and 73%, respectively) and significantly less Quaternary Alluvium (14% and 9%, respectively). For the flat classification, the percentage of Crystalline stations more than doubled, and the percent of Quaternary Alluvium was cut by greater than half, compared to the passing classification for both mHVSR and eHVSR. These changes in composition were more significant for eHVSR.

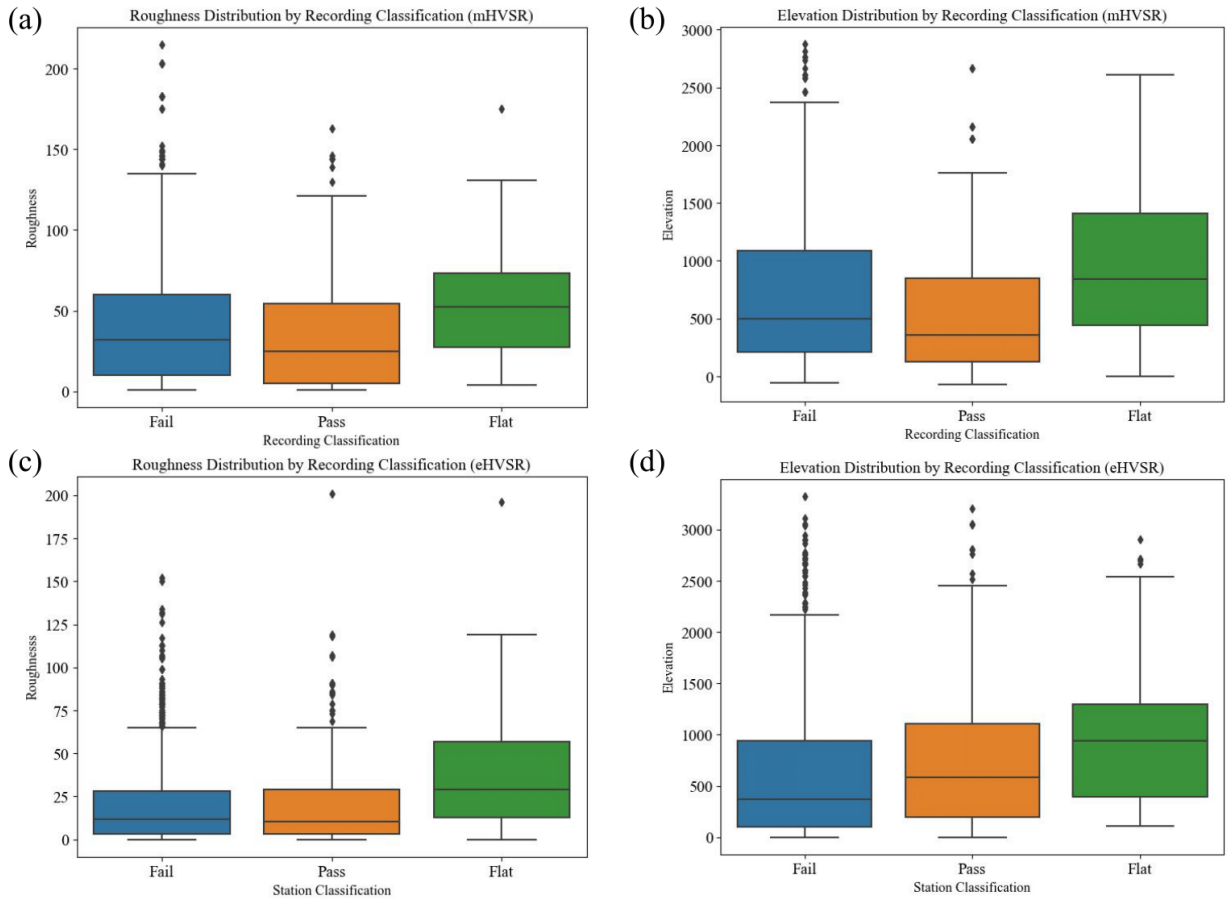

Figure 8. Distribution of roughness and elevation by the recording classifications for mHVSR (parts (a) and (b), respectively) and eHVSR (parts (c) and (d), respectively).

On average, stations with a flat classification have a higher elevation and roughness, they are also more likely to have crystalline surficial geology and less likely to have Quaternary alluvium surficial geology. This validates the effectiveness of the flat classification because stations that would have a consistently flat HVSR would be ones without impedance contrasts. Stations with flat classifications include many surficial geology types, but they are predominantly rock sites, which are crystalline and can have higher roughness and elevation (especially when they are located on mountain/hill sites). It will also be less likely that there are softer sediments like Quaternary alluvium at such sites, because there would be an impedance contrast in the underlying rock if such materials were encountered.

These results show that there is a significant difference in the geologic and topographic composition between flat stations and failing stations not classified as flat. This result further indicates the distinctness of the flat classification, and that it carries site information different from the other failing stations. The composition of the other failing stations align more closely with the passing stations. This result could indicate that while the peaks could not be identified using HVSR data, perhaps the peaks are not being captured due to variability from noise or environmental factors. For mHVSR stations with multiple recordings, 6 out of the 174 stations (3.4%) had a flat and a passing recording, whereas 53 out of the 174 stations (30.5%) had a failing and passing recording. This indicates that the flat classification improves the ability to identify sites without a resonance peak, compared to classifying all failed recordings this way. The same geologic and topographic trends are viewed across mHVSR and eHVSR data, indicating effectiveness of this method for both HVSR types.

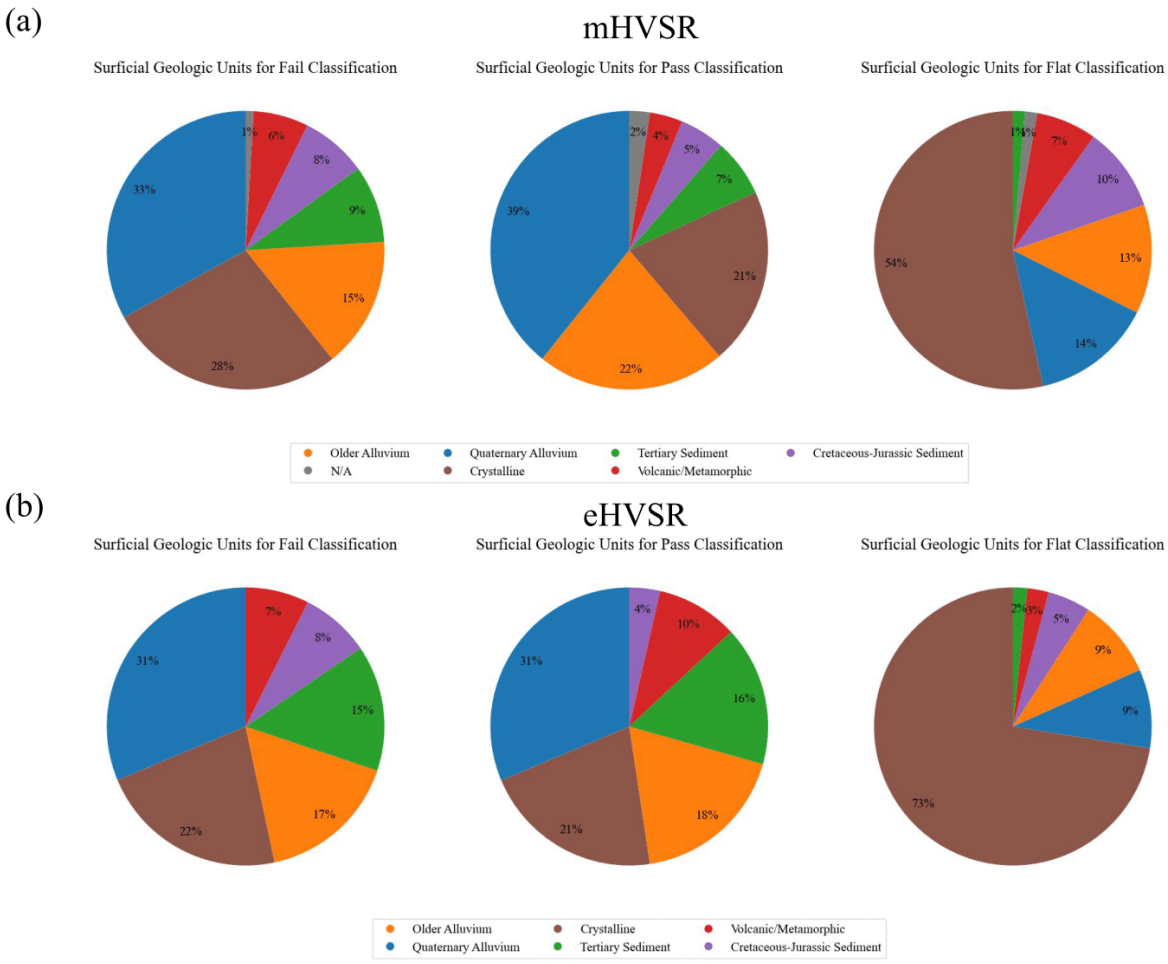

Figure 9. Surficial geologic make-up of the recording classifications for (a) mHVSR, and (b) eHVSR.

Including this flat HVSR classification in GMM development would capture the average amplification difference for sites without an impedance contrast compared to sites with a clear fundamental resonance frequency. Such as classification would be more accurate than simply classifying all failing stations as flat, as is evident by the differences between the groups and the consistency of the classification for mHVSR stations with multiple recordings. For the remainder of this study, only the flat and passing recordings are used due to the lack of conclusive evidence about site characterization from the failed recordings. We will handle HVSR measurements for use with GMMs as follows: implement correction terms for flat and passing recordings, but apply no correction for failing stations due to a lack of reliable results for the site.

Classification Consistency Between mHVSR and eHVSR

In this section, we examine to what extent eHVSR and mHVSR produce similar results across California, to determine how both datasets can be used to inform GMMs. We compare mHVSR recordings within the passing and flat classifications to eHVSR results at the same stations. Failed recordings are not considered here due to their insufficient information, as described previously. There were 92 mHVSR recordings across 65 stations where a passing or flat eHVSR result was obtained at the same stations. These 92 mHVSR/eHVSR recording pairs were analyzed to see how often they matched. Pairs were determined to be a match if (a) they are both flat, or (b) they both pass and the identified peak eHVSR frequency is within half to twice the mHVSR peak frequency. Across the set of 92 pairs, there were 58 pairs (64%) that matched using these criteria.

To understand when eHVSR matches mHVSR various prior conditions were analyzed, with the following results described here and shown in Figure 10:

(i.) Given that the eHVSR passes, there is a 75% probability that the mHVSR passes and matches.
(ii.) Given that eHVSR is flat, there is a 45% probability that the mHVSR is flat.
(iii.) Given that the mHVSR passes, there is a 59% probability that the eHVSR passes and matches.
(iv.) Given that mHVSR is flat, there is a 83% probability that the eHVSR is flat.
(v.) Given that the mHVSR and eHVSR pass, there is a 79% probability that the peak frequencies match.

These results indicate that the flat classification for eHVSR is not indicative of a flat mHVSR, resulting in low matching rates for conditions (ii) and (iii). However, the flat classification from mHVSR is indicative of a truly flat HVSR, evident by the eHVSR also being flat 83% of the time. Based on this result, we find that eHVSR too often classifies sites as flat, but the mHVSR flat classification is more universal. This finding is consistent with results from previous studies that showed when the mHVSR failed to identify a clear resonance, it was an indicator that the eHVSR is likely to be flat (Vantassel et al., 2024). However, the converse was not true: the lack of an eHVSR resonance was not a good indicator of the lack of an mHVSR resonance (Vantassel et al., 2024). It is more difficult to obtain a passing classification using eHVSR data in California; this means that the passing classifications are more reliable from eHVSR, with some error (25% in this study), but the flat classifications from eHVSR are not reliable when comparing to mHVSR.

Flat results from mHVSR are consistent with eHVSR at the same site, and have a clear distinction from passing and failing recordings, as demonstrated in the previous section. A flat classification for mHVSR

data allows for the fitting of a correction factor to GMMs that could be applied if a flat mHVSR is obtained at a site. However, flat-classified stations from eHVSR should not be included when fitting this correction factor.

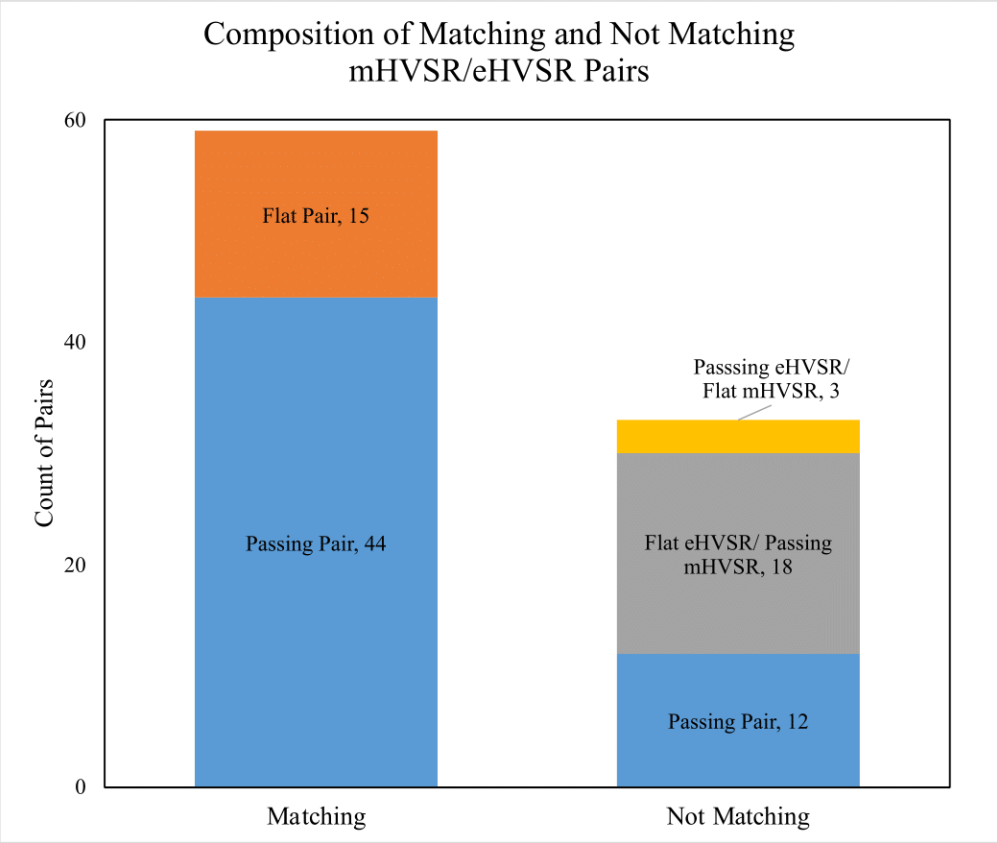

Figure 10. mHVSR/eHVSR pairs that matched and those that did not match, separated by the classification of the data in each pair.

Parameter Consistency within mHVSR Stations

We evaluate the consistency of the fundamental resonance peak frequency, peak amplitude, and the half-power bandwidth parameters for stations with multiple mHVSR recordings. For a parameter to be beneficial in a GMM, it would need to carry repeatable, consistent information for a site. There are 48 mHVSR stations with multiple passing recordings. The stations identified each have a range of two to four passing recordings.

To first assess the consistency of the three HVSR parameters, all the unique pairs of recordings within each station were identified; this procedure resulted in 92 mHVSR recording pairs. Figure 11 shows the fundamental resonance frequency, peak amplitude, and half-power bandwidth parameters for one mHVSR recording against its pair at the station. The peak frequencies show minimal scatter at frequencies below 4 Hz, but become less consistent across recordings as the frequency increases above 4 Hz. For peak amplitudes, the amplitudes tend to fall within a tight range of 2 to 6, and there is some scatter within this range. For HPB, there is scatter when high HPB values are reported, and these values are not repeatable; no HPB value above 4 Hz appeared consistent with other values at the site.

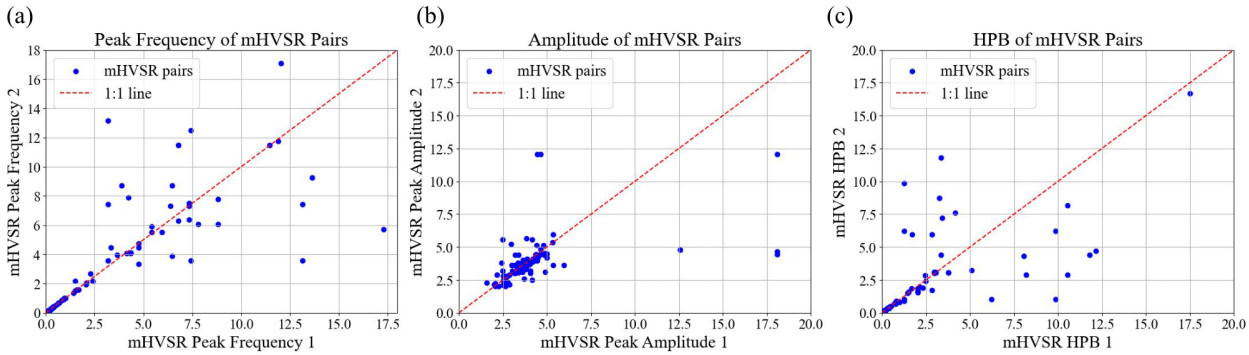

Figure 11. Peak fundamental resonance frequency (Hz), peak amplitude, and HPB (Hz) for mHVSR site pairs.

To conduct a more quantitative analysis, the average coefficient of variation (CV, computed as the standard deviation normalized by the mean) for fundamental resonance frequency, amplitude, and HPB was computed across the 48 stations with multiple passes. The CV is 0.13 for the fundamental resonance frequency and 0.14 for peak amplitude. Although the CV for amplitude is similar to that of fundamental resonance frequency, amplitude covers a smaller range, so this variability could be problematic for model use. The HPB has the largest CV at 0.22; however, the CV reduces to 0.10 if values above 4 Hz are removed from the dataset.

These metrics validate that the mHVSR fundamental resonance frequency is a consistent measure when it can be obtained at a site. HPB is also a consistent measure, provided it is only used when it falls below 4 Hz. For amplitude, the CV was not significantly higher than that of frequency or HPB; however, because of the small range amplitude covers, it may not be providing site information sufficient for a GMM.

Parameter Consistency Between mHVSR and eHVSR

We also explore the consistencies in peak frequency, peak amplitude, and HPB for recordings that passed for both eHVSR and mHVSR. There are 56 mHVSR recordings with a corresponding eHVSR pass at the same station. The eHVSR peak frequencies vs. mHVSR peak frequencies can be seen in Figure 12. The distribution closely follows the 1-to-1 line, with the exception of a few outliers. Figure 12 also shows the eHVSR vs. mHVSR amplitudes and HPBs. The amplitude shows a similar scatter pattern as the mHVSR pairs but has greater spread, and would present similar problems in GMM fitting due to the variability in the term and the small range of potential amplitudes. The HPB also shows more scatter than it did for mHVSR pairs. When only considering HPB values below 4 Hz, as is the recommendation from the mHVSR data, the values do show a consistent trend and lack the scatter cloud seen in the amplitude data, which could still make HPB a useful parameter in GMM development if the added uncertainty in eHVSR HPB is incorporated.

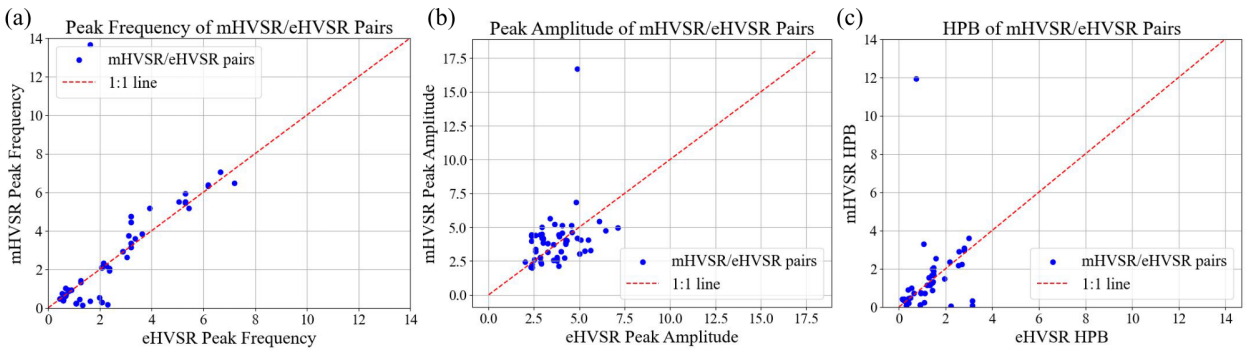

Figure 12. Peak fundamental resonance frequency (Hz), peak amplitude, and HPB (Hz) for eHVSR/mHVSR site pairs.

The above approach visualizes the consistency of each parameter, but to further quantify the distributions, we evaluated the Nash–Sutcliffe Efficiency Coefficient (E) for goodness of fit to the 1-to-1 line. The E value for peak frequency is 53%; however, this increases to 88% when the outlier at an mHVSR fundamental resonance frequency of 13.6 Hz (in the upper left corner of the plot, above the legend) is removed. Given the uncertainty previously discussed regarding the high mHVSR fundamental resonance frequencies, the agreement is likely closer to 88%, and 0.88 will be used for weighting the eHVSR frequencies in model fitting. For amplitude, the E value is 3.0%, indicating no agreement between observations and predictions. Even with the removal of the outlier at an mHVSR amplitude of 16.7, the E value decreases to -30%, which is consistent with the small range of the scatter seen in the data. The E value for HPB is 3.8%, again indicating no agreement between observations and predictions. However, when the HPB values above 4 Hz were removed, due to their unreliability as seen the mHVSR-only dataset, the E value increases to 33%. A weight of 0.33 will be used for eHVSR HPB in model fitting and only HPB values below 4 are used for model fitting and use. As discussed previously, a weight of one is used for the mHVSR data for model fitting in all cases.

Given these results, we use fundamental resonance frequencies and HPB values from passing eHVSRs to supplement mHVSR data when fitting GMMs, in order to utilize the added site coverage across the state of eHVSR data. The uncertainty in whether the eHVSR parameter matches the mHVSR parameter at a site is incorporated when fitting the model using the calculated E value as the weight. The amplitude from passing eHVSRs is not used when fitting an amplitude-based correction term due to the lack of consistency between eHVSR and mHVSR amplitudes.

HVSR-Based GMM Correction Term

Model Selection

Five linear HVSR-based correction factors for GMM site terms were evaluated. Three of these models were fit using parameters from only mHVSR data using OLS regression following Equation 3. The three models were each fit using a different HVSR parameter: fundamental resonance frequency, amplitude, and HPB. The other two models were fit using a combination of eHVSR data and mHVSR data, using WLS regression following Equation 3. The two models are for fundamental resonance frequency and HPB. A model fit to amplitude as the dependent variable using eHVSR and mHVSR data was not assessed due to the lack of agreement between mHVSR and eHVSR amplitude data, as discussed previously. All five models use only data from passing stations, and the HPB models use only HPB

values below 4 Hz. HPB values above 4 Hz were not considered for a correction factor due to their unreliability. From all five models, 20% of the passing mHVSR recordings were left out during model fitting in order to test the model performance on unseen data. The RMSE was calculated for each model on the left-out mHVSR data, and the results can be seen in Figure 13.

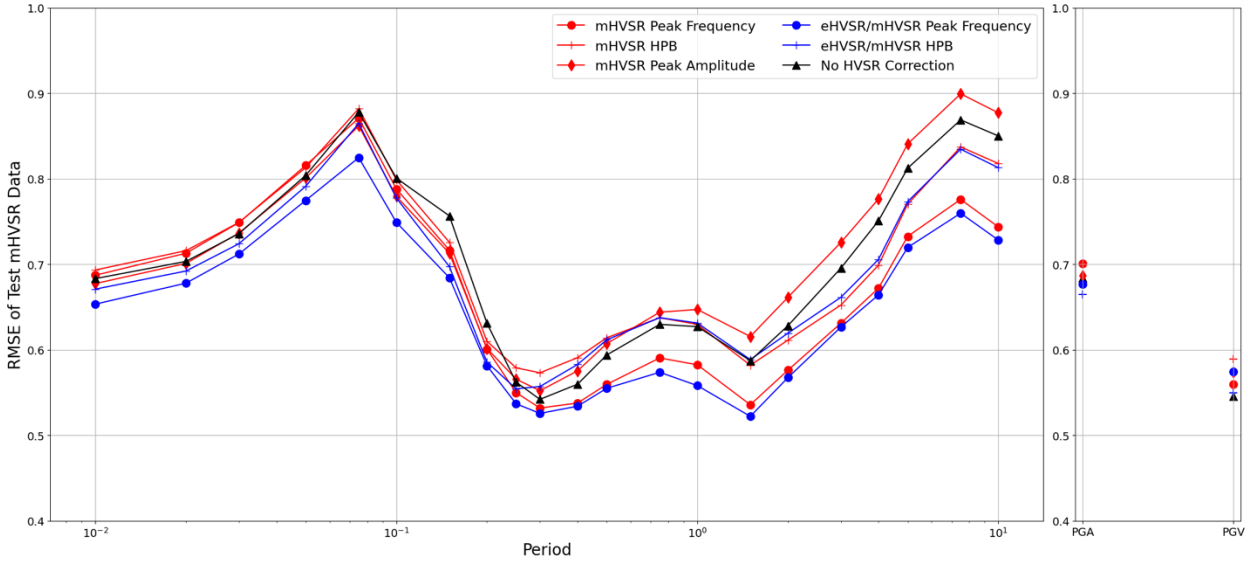

Figure 13. RMSE of the left-out mHVSR data for each of the five models evaluated.

The eHVSR- and mHVSR-fitted fundamental resonance frequency is the best linear HVSR term for passing stations because it has the lowest RMSE for the test set of mHVSR data for PGA, PGV, and all 21 periods evaluated. The correction term based on fundamental resonance frequency reduces the RMSE by an average of 7.2% compared to using no correction factor. Including eHVSR frequency data reduces the RMSE by an average of 3.0%, with the significant reduction occurring between periods 0.01 to 0.1 seconds (average of 4.9%), compared to only using mHVSR frequency data.

The correction factor for flat stations was also evaluated. The factor is a constant that can be applied to stations for which the mHVSR curve meets the flat criteria. To assess the accuracy of this flat correction factor, we fit the correction factor to the S2S values from 80% of the flat mHVSR recordings, and then tested using this factor for the remaining 20% of flat mHVSR recordings. Only mHVSR data were used to fit the flat HVSR correction factor because a flat result from eHVSR is not a reliable indicator of a flat mHVSR, as previously discussed.

The RMSE was calculated for each model on the left-out mHVSR data, and the results can be seen in Figure 14. In this figure, we also compare the result to the RMSE of the test data without a correction factor. Including a correction factor for the site term of flat stations results in a reduction of RMSE for the test set of mHVSR data. The average reduction in RMSE is 15.2%, with largest reduction occurring for spectral periods of 0.2 to 1.5 seconds, having an average reduction of 22.0%.

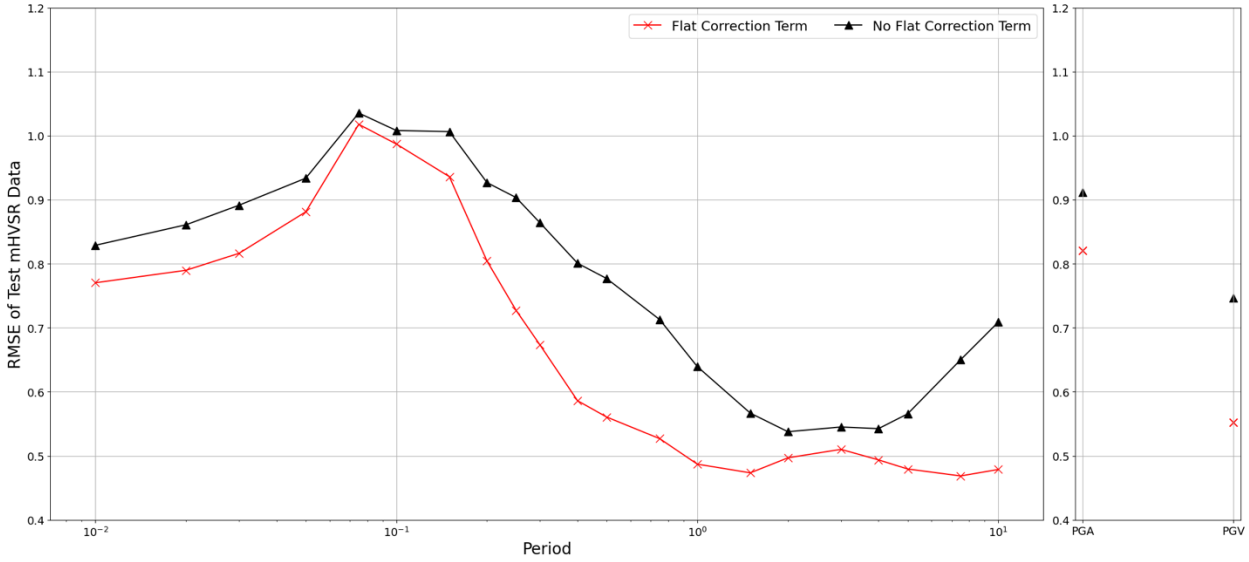

Figure 14. RMSE of the left-out mHVSR data for the flat correction term and no correction term.

To evaluate how the models perform in reducing variability in GMMs, in Figure 15 we compare the S2S variability of PGA, PGV, and PSAs across 21 periods from 0.01 to 10 seconds both with and without the HVSR correction term. Applying the optimal linear model for passing stations, the eHVSR and mHVSR fitted term for fundamental resonance frequency, and the flat correction factor for flat stations yields a reduction in standard deviation of S2S for the test mHVSR dataset as well. The average reduction in standard deviation of S2S across all periods is 10.9%.

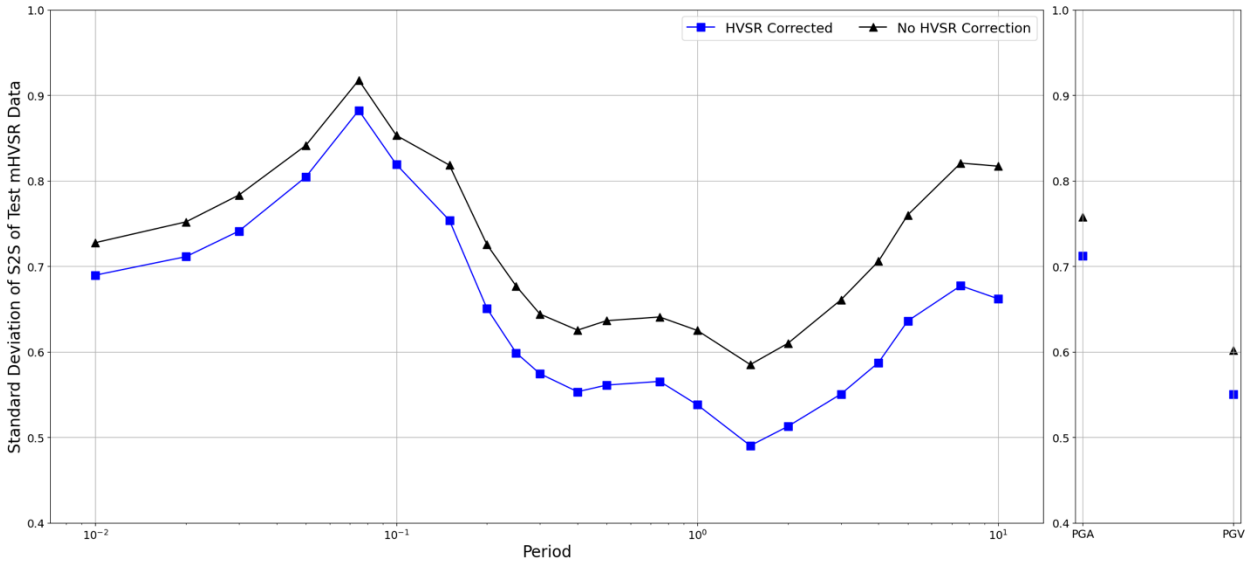

Figure 15. Comparison of between-site variability (standard deviation of S2S) for the test set of mHVSR data. The black line represents no HVSR correction, and the blue line represents the data with the correction applied to passing and flat stations.

Final HVSR Correction Term

Given the results of the validation process, we propose an HVSR-based correction factor for site terms that uses an eHVSR and mHVSR fitted WLS linear term for fundamental resonance frequency for passing stations and an mHVSR fitted correction factor for flat recordings. The inclusion of fundamental resonance frequency as a predictor approximates the site fundamental frequency to improve the site term of the GMM. Using both eHVSR and mHVSR data to fit the term provides a larger dataset that also covers a larger geographic area to fit a more generalizable model. The addition of the flat term allows for sites without a fundamental frequency to be corrected for this lack of impedance contrast at the site, improving site term calculation for these sites. The linear correction factor for passing sites and the constant correction factor for flat sites is expressed as

$$Y_j = \begin{cases} c_0 + c_1 X_{f_o,j}, & HVSR\ station\ claasification = pass \\ c_2, & HVSR\ station\ classification = flat \end{cases}, \quad (6)$$

where Y_j is the HVSR correction factor for the site, $X_{f_o,j}$ is the fundamental resonance frequency of the site, c_0 is the period-dependent intercept for the passing stations, c_1 is the period-dependent slope for the passing stations, and c_2 is the period-dependent constant term for flat stations. The coefficients by period can be found in the Appendix to this report. The coefficients provided were refit to the entire dataset, including the testing mHVSR dataset, to produce more representative coefficients.

The standard deviations of S2S for PGA, PGV, and PSAs across 21 periods from 0.01 to 10 seconds were calculated for all of the stations with passing or flat mHVSR curves, after applying the correction factor in Equation 6. In Figure 16, we compare the standard deviation of S2S at these stations both with and without the HVSR-based correction term. The average reduction in standard deviation of S2S with the correction factor is 5.2%. The RMSE was also calculated and has an average reduction of 6.8%, as shown in Figure 17.

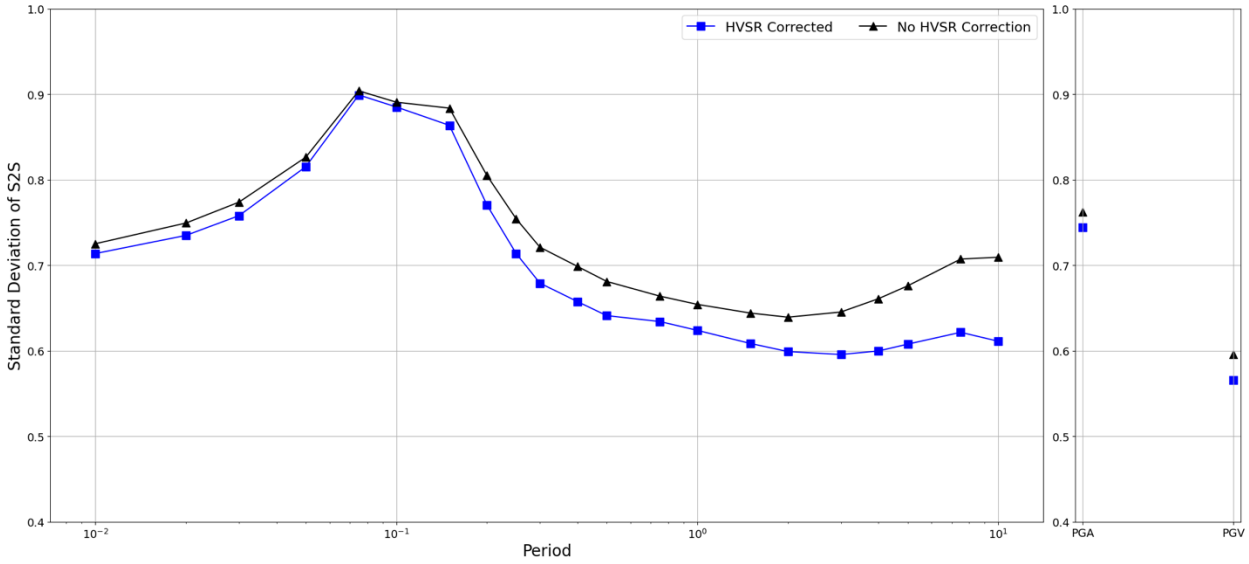

Figure 16. Comparison of between site variability (standard deviation of S2S) for the set of stations with mHVSR data (211 passing stations and 76 flat stations). The black line represents no HVSR correction, and the blue line represents the data with the correction applied to passing and flat stations.

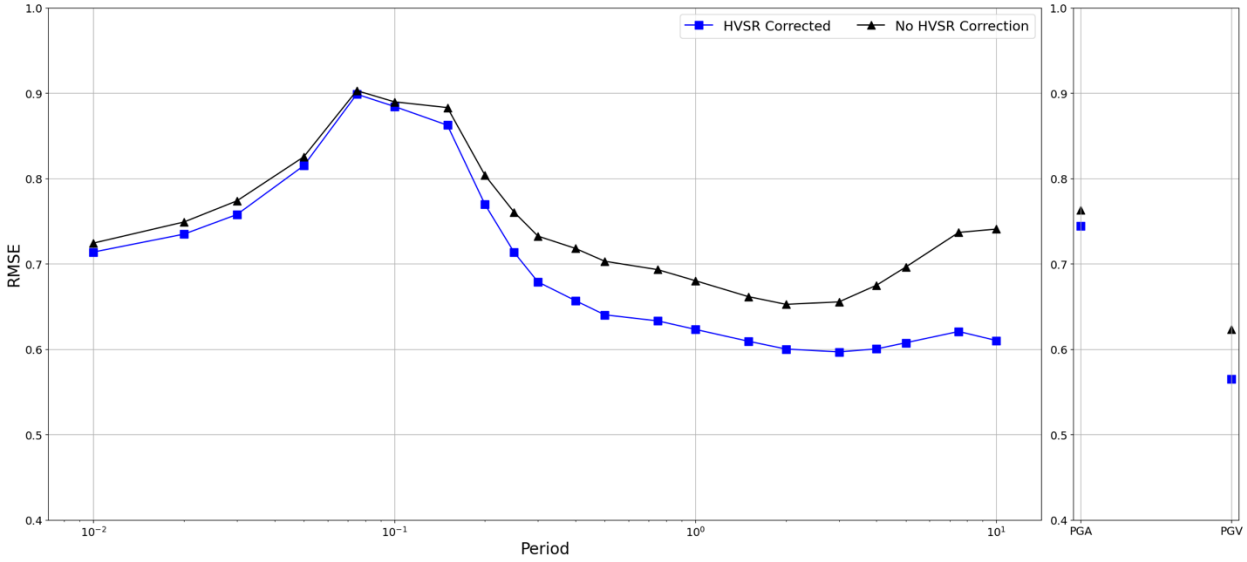

Figure 17. Comparison of RMSE for the set of stations with mHVSR data (211 passing stations and 76 flat stations). The black line represents no HVSR correction, and the blue line represents the data with the correction applied to passing and flat stations.

4. Discussion

The developed HVSR-based correction term allows for updating to non-ergodic geospatial-based models by informing them with local geotechnical information when it is available. Our novel approach of using a strict criterion for classification of flat HVSR recordings and including a correction factor for flat HVSR stations improves the site term calculation for stations without a fundamental resonance peak. Including both eHVSR and mHVSR data also improves the correction factor performance on mHVSR data by fitting the model with a larger dataset that covers a greater geographic region.

This model is designed for use as a site term correction factor in California and provides improvements to geospatial-based site terms through local geotechnically-informed corrections. The methodology used to develop the model could also be applied in other regions. An HVSR correction factor would be beneficial in areas with a strong impedance contrast that may not be fully captured in the model. The development of a comparable model in other regions is constrained by the availability of HVSR data. Modifying methods to account for uncertainty between eHVSR and mHVSR that may vary by region will be an important step for model development in other areas.

5. Conclusions

We developed a site term correction factor from HVSR data for California. The model is developed for PGA, PGV, and 5%-damped PSA from 0.01 to 10 s, using mHVSR data from the Wang et al. (2022) Horizontal-to-Vertical Spectral Ratio Database and eHVSR data from the Ji et al. (2022) DesignSafe Ground Motion Database.

The optimal HVSR-based site term is developed using a combination of mHVSR and eHVSR data. The HVSR data was processed and classified as either passing the SESAME criteria and having a clear peak

identified, flat (failing SESAME criteria 1 and 2, and having a peak HVSR amplitude below 1.5), or failing to be identified as either passing with a clear peak or flat. The flat designation applied here is a new categorization for HVSR data that separates (a) flat stations with no resonance from (b) stations that fail to have a peak identified because of too much noise in the data. Correction factors are developed for use with GMM site terms for sites with a passing HVSR and sites with a flat HVSR.

Two sets of models were assessed, one fit using only mHVSR data, and one fit using mHVSR and eHVSR data, across three HVSR parameters (fundamental resonance frequency, amplitude, and half-power bandwidth) for their ability to reduce site-to-site variability (S2S). Weighted Least Squares regression is used to fit the models that use both eHVSR and mHVSR data to account for variability between eHVSR and mHVSR data. The fundamental resonance frequency from the passing mHVSR and eHVSR stations performed the best, in terms of the lowest RMSE across a test set of mHVSR data. This term is used as the linear portion of the HVSR correction factor applicable to sites with a passing peak from HVSR. The flat stations from the mHVSR dataset are used to fit a constant correction factor for flat stations.

The HVSR correction factor for passing and flat sites results in reduction in site-to-site variability (S2S) compared to a geospatial non-ergodic model for California that uses continuous geospatial variables. The proposed correction term provides local geotechnical information to enhance the accuracy of the GMM site term. HVSR is a simple and low-cost method for analyzing site fundamental frequency, making it an accessible addition to enhance GMMs when it can be measured at a site or is already available. Additionally, this model includes a correction for sites designated as having flat HVSRs, instead of considering these sites to be failed. The inclusion of sites with flat HVSRs allows for more information to be drawn from HVSRs to further reduce GMM residuals.

The HVSR-based correction factor is intended to capture the effects of the fundamental frequency on the site term and improve ground motion estimates across California. The approach of using passing and flat HVSRs and combining mHVSR and eHVSR data could be applied in other regions outside of California, and would be particularly beneficial in regions with strong impedance contrast and available mHVSR data. We propose a correction factor for GMM site terms derived from both mHVSR and eHVSR data to be used when HVSR data can be collected or is available to improve site term calculation.

6. Data and Resources

The earthquake ground-motions were obtained from the Ji et al. (2022) DesignSafe Ground Motion Database (https://www.designsafe-ci.org/data/browser/public/designsafe.storage.published/PRJ-3031v2?doi=10.17603%2Fds2-syc5-nk92&version=2). The ground-motion data were processed to obtain HVSR curves using *hvsrpy* (Vantassel, 2020). *Hvsrpy* is an open-source python package for processing eHVSR and mHVSR and is available at https://github.com/jpvantassel/hvsrpy. The data were processed to obtain ground motion predictions using the BSSA14 GMM (Boore et al., 2014) coded and available at https://github.com/bakerjw/GMMs/blob/master/gmms/bssa_2014_active.m modified with the site term reported in Roberts et al. (2024).

The mHVSR curves were obtained from the Wang et al. (2022) Horizontal-to-Vertical Spectral Ratio Database, available via DesignSafe at https://www.designsafe-

ci.org/data/browser/public/designsafe.storage.published/PRJ-3085. The mHVSR parameters were determined using using *hvsrpy* (Vantassel, 2020), available at https://github.com/jpvantassel/hvsrpy.

The analysis of the results from the processed HVSR data was performed using the open-source environment Python (Python Software Foundation, 2023), available at https://www.python.org.

This project involves processing of electronic data (sources described above) and modeling results. No new geotechnical or seismic data was collected as a part of this project. This project will be published in at least one journal article, and the data generated will appear as an electronic supplement to the published journal article(s).

7. Bibliography

The following publications resulted from this project. At least one manuscript is currently being prepared for submission to a peer-reviewed journal, and an abstract has been approved for an upcoming conference where results from this project will be presented. The results from this project were also presented at one other conference, resulting in a conference abstract:

Roberts, M., Baise, L., Nie, S., Kaklamanos, J., & Zhan, W. (2024). Geospatial Variable Based Site Terms for Nonergodic Ground Motion Models, *2024 Annual Meeting of the Seismological Society of America*, Anchorage, Alaska, 29 April – 3 May 2024 (abstract printed in *Seismological Research Letters*, Vol. 95, No. 5).

Roberts, M., Baise, L., Nie, S., Kaklamanos, J., & Zhan, W. (2024). *Geologically Informed Non-Ergodic Site Effects Model for California* [Manuscript in progress]. Civil and Environmental Engineering, Tufts University.

Roberts, M., Baise, L., Nie, S., Kaklamanos, J., Zhan, W., & Meyer, E. (2024). HVSR Based Site Terms to Enhance Nonergodic Ground Motion Models in California, *2024 Annual Meeting of the American Geophysical Union*, Washington, D.C., 9-13 December 2024.

8. References

Abrahamson, N. A., & Youngs, R. R. (1992). A stable algorithm for regression analyses using the random effects model. *Bulletin of the Seismological Society of America*, 82 (1), 505-510.

Boore, D. M., Stewart, J. P., Seyhan, E., & Atkinson, G. M. (2014). NGA-West2 equations for predicting PGA, PGV, and 5% damped PSA for shallow crustal earthquakes. *Earthquake Spectra*, 30 (3), 1057-1085.

Braganza, S., Atkinson, G.M., Ghofrani, H., Hassani, B., Chouinard, L., Rosset, P., Motazedian, D., & Hunter, J. (2016). Modeling Site Amplification in Eastern Canada on a Regional Scale. *Seismological Research Letters*, 87 (4), 1008–1021.

Carpenter, S. N., Wang, Z., & Woolery, E. W. (2020). An Evaluation of Linear Site-Response Parameters in the Central and Eastern United States and the Importance of Empirical Site-Response Estimations. *Bulletin of the Seismological Society of America*, 110 (2), 489–507.

Carpenter, N. S., Wang, Z., Woolery, E. W., & Rong, M. (2018). Estimating Site Response with Recordings from Deep Boreholes and HVSR: Examples from the Mississippi Embayment of the Central United States. *Bulletin of the Seismological Society of America*, 108 (3A), 1199–1209.

Cox, B. R., Cheng, T., Vantassel, J. P., & Manuel, L. (2020). A statistical representation and frequency-domain window-rejection algorithm for single-station HVSR measurements. *Geophysical Journal International*, 221(3), 2170–2183.

Chao, S. H., Lin, C. M., Kuo, C. H., Huang, J. Y., Wen, K. L., & Chen, Y. H. (2021). Implementing horizontal-to-vertical Fourier spectral ratios and spatial correlation in a ground-motion prediction equation to predict site effects. *Earthquake Spectra*, 37 (2), 827–856.

Danielson, J. J. & Gesch, D. B. (2011). Global multi-resolution terrain elevation data 2010 (GMTED2010) (No. 2011-1073). *US Geological Survey*.

Gallipoli, M. R. & Mucciarelli, M. (2009). Comparison of Site Classification from VS_{30}, VS_{10}, and HVSR in Italy. *Bulletin of the Seismological Society of America*, 99 (1), 340–351.

Guy, M., Patton, J., Fee, J. M., Hearne, M., Martinez, E. M., Ketchum, D., Worden, C. B., Quitoriano, V., Hunter, E. J., Smoczyk, G. M., & Schwarz, S. (2015). National Earthquake Information Center systems overview and integration: *U.S. Geological Survey Open-File Report* 2015–1120, 25 p.,

Hassani, B., & Atkinson, G. M. (2016). Site-effects model for central and eastern North America based on peak frequency. *Bulletin of the Seismological Society of America*, 106 (5), 2197-2213.

Hassani, B., & Atkinson, G. M. (2018). Site-effects model for Central and Eastern North America based on peak frequency and average shear-wave velocity. *Bulletin of the Seismological Society of America,* 108 (1), 338-350.

Hassani, B., Yong, A., Atkinson, G. M., Feng, T., & Meng, L. (2019). Comparison of Site Dominant Frequency from Earthquake and Microseismic Data in California. *Bulletin of the Seismological Society of America*, 109 (3), 1034-1040.

Ji, C., Cabas, A., Kottke, A., Pilz, M., Macedo, J., & Liu, C. (2022). A DesignSafe Ground Motion Database: time series, engineering metrics, and site metadata, in A DesignSafe Ground Motion Database: time series, engineering metrics, and site metadata [Version 2]. *DesignSafe-CI*.

Kawase, H., Nagashima, F., Nakano, K., & Mori, Y. (2019). Direct evaluation of S-wave amplification factors from microtremor H/V ratios: Double empirical corrections to "Nakamura" method. *Soil Dynamics and Earthquake Engineering*, 126, 105067.

Konno, K., & Ohmachi, T. (1998). Ground-motion characteristics estimated from spectral ratio between horizontal and vertical components of microtremor. *Bulletin of the Seismological Society of America*, 88 (1), 228-241.

Lermo, J., & Chávez-García, F. J. (1993). Site effect evaluation using spectral ratios with only one station. *Bulletin of the seismological society of America*, 83 (5), 1574-1594.

Nakamura, Y. (1989). A Method for Dynamic Characteristics Estimation of Subsurface using Microtremor on the Ground Surface. *Railway Technical Research Institute*, 30 (1), 25–33.

Nash, J. E., & Sutcliffe, J. V. (1970). River flow forecasting through conceptual models: Part I, a discussion of principles, *Journal of Hydrology*, 10, 282–290.

Nogoshi, M., & Igarashi, T. (1971). On the amplitude characteristics of microtremor, Part II. *Journal of the seismological society of Japan*, 24, 26-40.

Roberts, M., Baise, L., Nie, S., Kaklamanos, J., & Zhan, W. (2024). Geologically Informed Non-Ergodic Site Effects Model for California [Manuscript in progress]. *Civil and Environmental Engineering, Tufts University.*

SESAME. (2004). Guidelines for the Implementation of the H/V Spectral Ratio Technique on Ambient Vibrations Measurements, Processing, and Interpretation. *European Commission - Research General Directorate*, 62.

Vantassel, J. P., Ilgac, M., Zekkos, A. A., Yong, A., Hassani, B., & Martin, A. J. (2024). Are the Horizontal-to-Vertical Spectral Ratios of Earthquakes and Microtremors the Same?. *Bulletin of the Seismological Society of America*, in press, https://doi.org/10.1785/0120240039.

Vantassel, J. (2020). jpvantassel/hvsrpy: latest (Concept). Zenodo. http://doi.org/10.5281/zenodo.3666956.

Wang, P (2021). wltcwpf/hvsrProc: First release (Version v1.0.0). Zenodo. http://doi.org/10.5281/zenodo.4724141.

Wang, P., Zimmaro, P., & Stewart, J. (2021). Horizontal-to-Vertical Spectral Ratio Database Access and Analysis, in Horizontal-to-Vertical Spectral Ratio Database Access and Analysis [Version 2]. *DesignSafe-CI*.

Wathelet, M., Chatelain, J. L., Cornou, C., Giulio, G. D., Guillier, B., Ohrnberger, M., & Savvaidis, A. (2020). Geopsy: A user-friendly open-source tool set for ambient vibration processing. *Seismological Research Letters*, 91 (3), 1878-1889.

Wills, C. J., Gutierrez, C. I., Perez, F. G., & Branum, D. M. (2015). A next generation VS30 map for California based on geology and topography. *Bulletin of the Seismological Society of America*, 105 (6), 3083-3091.

Yazdi, M., Anderson, J. G., & Motamed, R. (2023). Reducing the uncertainties in the NGA-West2 ground motion models by incorporating the frequency and amplitude of the fundamental peak of the horizontal-to-vertical spectral ratio of surface ground motions. *Earthquake Spectra*. 39 (2), 1088-1108.

Zhu, C., Pilz, M., & Cotton, F. (2020). Evaluation of a novel application of earthquake HVSR in site-specific amplification estimation. *Soil Dynamics and Earthquake Engineering*, 139, 106301.

Appendix

Table A.1 Coefficients by period for the HVSR-based correction term from Equation 6.

Period	c_0	c_1	c_2
PGA	0.0891	0.0029	-0.3383
PGV	0.0549	-0.0262	-0.4659
PSA 0.01 s	0.0846	0.0090	-0.2513
PSA 0.02 s	0.0894	0.0056	-0.2920
PSA 0.03 s	0.0921	0.0039	-0.3132
PSA 0.05 s	0.0812	0.0097	-0.2706
PSA 0.075 s	0.0579	0.0246	-0.1552
PSA 0.1 s	0.0841	0.0190	-0.1759
PSA 0.15 s	0.1463	0.0108	-0.2985
PSA 0.2 s	0.1745	-0.0057	-0.3934
PSA 0.25 s	0.1583	-0.0222	-0.4701
PSA 0.3 s	0.1689	-0.0343	-0.4800
PSA 0.4 s	0.1655	-0.0493	-0.4808
PSA 0.5 s	0.1768	-0.0582	-0.4700
PSA 0.75 s	0.1200	-0.0600	-0.4540
PSA 1 s	0.1012	-0.0597	-0.4380
PSA 1.5 s	0.1090	-0.0609	-0.4103
PSA 2 s	0.1208	-0.0600	-0.3927
PSA 3 s	0.1323	-0.0572	-0.3995
PSA 4 s	0.1427	-0.0588	-0.4607
PSA 5 s	0.1448	-0.0606	-0.5137
PSA 7.5 s	0.1709	-0.0672	-0.6057
PSA 10 s	0.2026	-0.0715	-0.6409